A Delayless Subband Adaptive Filter Architecture

Dennis R. Morgan, *Senior Member, IEEE*, and James C. Thi, *Member, IEEE*

Abstract—**Some adaptive signal processing applications, such as wideband active noise control and acoustic echo cancellation, involve adaptive filters with hundreds of taps. The computational burden associated with these long adaptive filters precludes their use for many low-cost applications. In addition, adaptive filters with many taps may also suffer from slow convergence, especially if the reference signal spectrum has a large dynamic range. Subband techniques have been recently developed for adaptive filters to solve these problems. However, the conventional approach is ruled out for many applications because delay is introduced into the signal path. This paper presents a new type of subband adaptive filter architecture in which the adaptive weights are computed in subbands, but collectively transformed into an equivalent set of wideband filter coefficients. In this manner, signal path delay is avoided while retaining the computational and convergence speed advantages of subband processing. An additional benefit accrues through a significant reduction of aliasing effects. An example of the general technique is presented for a 32-subband design using a polyphase FFT implementation. For this example, the number of multiplies required are only about one-third that of a conventional fullband design with zero delay, and only slightly greater than that of a conventional subband design with 16 ms delay.**

I. Introduction

ADAPTIVE filtering techniques are now in widespread use for a number of applications such as adaptive arrays, adaptive noise cancellation, adaptive signal enhancement, adaptive modeling, adaptive equalization, and adaptive echo cancellation [1]. More recently, these techniques have also been applied to the expanding field of active noise control [2].

Some adaptive signal processing applications involve adaptive filters with hundreds of taps. Examples of such applications include wideband active noise control and acoustic echo cancellation, both of which are characterized by long impulse responses. The computational burden associated with these long adaptive filters precludes their use for many low-cost applications. With the advent of digital signal processing chips, this burden has been substantially reduced, yet many interesting applications are still beyond the reach of today's technology. In addition to computational complexity, adaptive filters with many taps may also suffer from long convergence time, especially if the reference signal spectrum has a large dynamic range. This problem is well understood to relate to a wide spread of eigenvalues associated with the reference signal covariance matrix [1].

Subband techniques have been recently developed for adaptive filters to solve the above problems [3]. Processing the signals in subbands has a twofold advantage: the computational burden is reduced by approximately the number of subbands, since both the number of taps and weight update rate can be decimated in each subband; also, faster convergence is possible because the spectral dynamic range is greatly reduced in each subband. Notable success has been achieved using this method for acoustic echo cancellation [4].

The disadvantage of conventional subband adaptive filters is that delay is introduced into the signal path by virtue of the bandpass filters used to derive the subband signals. For active noise control, delay seriously limits the bandwidth over which good cancellation can be achieved. For acoustic echo cancellation, the perceptual effects of incomplete echo cancellation are exacerbated by transmission delay, and permissible limits are strictly controlled in long-haul transmission systems. Thus, conventional subband adaptive filtering is precluded for applications requiring low delay.

A different approach to reducing the computational burden of long adaptive filters is to employ block transforms and perform all signal processing in the frequency domain [3]. However, straightforward application of this technique results in a substantial signal path delay corresponding to one block length. A variation of the block transform approach that eliminates signal path delay has been proposed by VanGerwen for an acoustic echo canceler [5]. In [5], the adaptive filter weights are computed in the frequency domain but are then transformed to the equivalent time-domain coefficients of a wideband filter that produces the actual cancellation signal. A similar technique was independently conceived for line echo cancellation in full-duplex data transmission [6]. One disadvantage of the block transform approach is a long block delay associated with the adaptive weight update, which can compromise performance in rapidly-changing environments. Also, this technique is not directly usable for applications that do not have ready access to the cancellation summing node, such as active noise control. We note that [5] and [6] are not subband adaptive filters in the usual sense since all adaptive processing takes place in the frequency domain.

This paper presents a new type of subband adaptive filter architecture that avoids signal path delay while retaining the computational and convergence speed advantages of subband processing. The delayless attribute of the technique is similar

Manuscript received October 15, 1993; revised March 13, 1995. The associate editor coordinating the review of this paper and approving it for publication was Dr. Virginia L. Stonick.

D. R. Morgan is with the Acoustics Research Department, AT&T Bell Laboratories, Murray Hill, NJ 07974-0636 USA.

J. C. Thi was with AT&T Bell Laboratories, Arlington, VA 22202 USA. He is now with Rockwell International, Newport Beach, CA 92658-8902 USA.

IEEE Log Number 9412628.

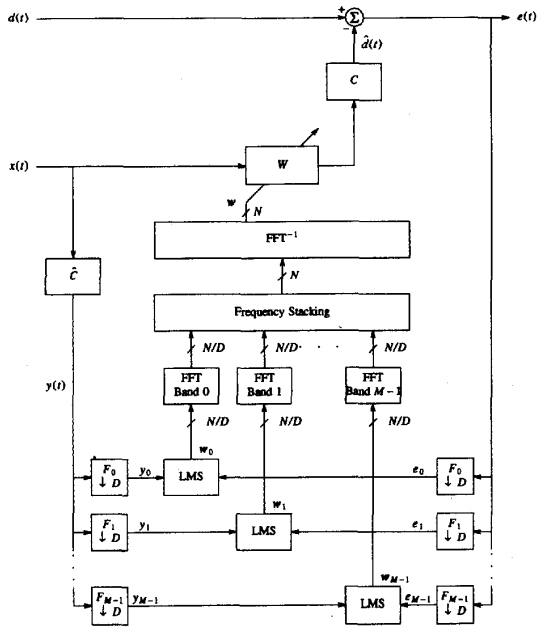

Fig. 1. Delayless subband adaptive filter using the FXLMS algorithm.

in spirit to the transform approaches discussed above: the adaptive weights are computed in subbands and then transformed to an equivalent wideband filter. However, the substance of this paper differs from [5] and [6] in that subband signals are processed in the time domain, rather than employing pure frequency-domain transforms. The efficiency and versatility of the subband architecture confer unique advantages over [5] and [6], such as the ability to independently vary the number of taps in each subband to optimize computational complexity and convergence speed. Moreover, this configuration can be used in applications that do not have direct access to the summing node, due to an intervening transfer function. With respect to conventional subband designs, an additional benefit of the new technique accrues through a significant reduction of aliasing effects caused by subband filter decimation.

Section II presents the general technique for arbitrary subband filters. A particularly efficient implementation using the polyphase FFT technique is discussed in Section III, and an example is developed for a 32-subband design. This design is then specialized to two applications in Section IV: delayless subband active noise control and delayless subband acoustic echo cancellation. Computational requirements are discussed in Section V.

II. General Technique

Fig. 1 shows a general block diagram of the delayless subband adaptive filter. The reference signal $x(t)$ is filtered by W and couples through the cancellation path transfer function C to cancel the disturbance signal $d(t)$. The intention is to adjust the coefficients of the wideband FIR filter W in order to minimize the residual error $e(t)$ in a mean-square sense. This general technique is exemplified by the active noise control problem, where C is an electromechanical or electroacoustic transfer function from a secondary source to the error sensor. Referring to Fig. 1, the wideband error signal is written as

$$e(t) = d(t) - c(t) * \left[\boldsymbol{w}^T(t)\boldsymbol{x}(t)\right], t = 0, 1, 2, \cdots \quad (1)$$

where $c(t)$ is the impulse response of the cancellation path filter, $*$ denotes convolution, $\boldsymbol{w}(t)$ is a vector of N wideband adaptive weights, and $\boldsymbol{x}(t) \equiv [x(t), x(t-1), \cdots, x(t-N+1)]^T$ is a vector comprising the N most recent reference samples, with superscript T denoting transpose.

In adaptive noise cancellation applications, there is no cancellation path transfer function ($C = 1$), and the LMS algorithm [1] is commonly used to adapt the filter coefficients. The more general technique for an arbitrary cancellation path transfer function C involves a modified version of the LMS algorithm that compensates for the cancellation path transfer function C by filtering the reference signal by the cancellation path transfer function estimate $\hat{C}$ [7]. This method was independently developed in [8], and is now commonly referred to as the "filtered-x" LMS (FXLMS) algorithm [1], which was independently conceived in the context of adaptive control systems [9]. The FXLMS algorithm and its IIR generalization have figured prominently in recent active noise control research [10]–[13].

In this paper, the wideband weight $\boldsymbol{w}$ is developed as a transformation of filtered-x derived subband weights, thereby eliminating any delay associated with the cancellation signal. The filtered reference signal $y(t)$ and error signal $e(t)$ are decomposed into sets of subband signals using single-sideband bandpass filters $F_0, F_1, \cdots, F_{M-1}$ that span the signal bandwidth. In each subband, the signals are decimated by a factor D (possibly after appropriate band shifting) and the subband adaptive weights are computed by the complex LMS algorithm, as detailed in Fig. 2(a). The adaptive weights in each subband are then transformed into the frequency domain, appropriately stacked, and inverse transformed to obtain the wideband filter coefficients.

For N wideband adaptive weights and a decimation factor D, there are N/D adaptive weights for each subband. The update of the subband adaptive weights depicted in Fig. 2(a) from time t to (decimated) time $t + D$ is expressed mathematically for each of the M subbands as

$$\boldsymbol{w}_m(t+D) = \boldsymbol{w}_m(t) + \mu \boldsymbol{y}_m^*(t) e_m(t), m = 0, 1, \cdots, M-1 \quad (2)$$

where $\boldsymbol{w}_m$ is a vector of N/D subband adaptive weights, μ is the adaptive step size, $\boldsymbol{y}_m(t) \equiv [y_m(t), y_m(t-D), \cdots, y_m(t-N+D)]^T$ is a vector comprising the N/D most recent (decimated) samples of the subband filtered reference signal with superscript $*$ denoting complex conjugate, and $e_m(t)$ is the subband error signal.

For real signals, the wideband filter coefficients are real and only half of the subbands need to be processed, corresponding to the positive frequency components of the wideband filter response; the other half of the response is formed in complex

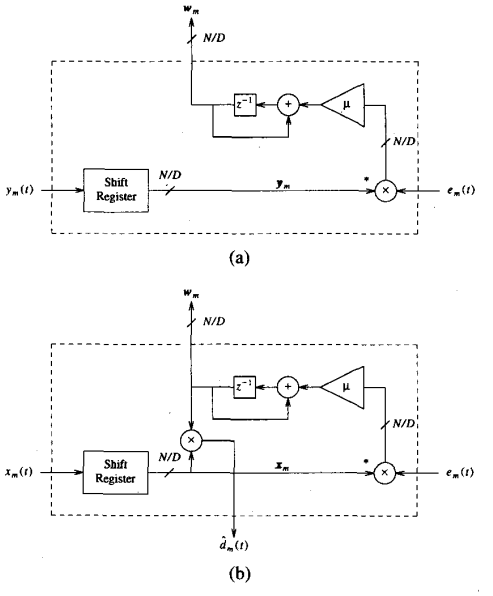

Fig. 2. Complex LMS algorithm. (a) Weight computation only, for closed-loop operation. (b) Weight computation and convolution, for open loop operation.

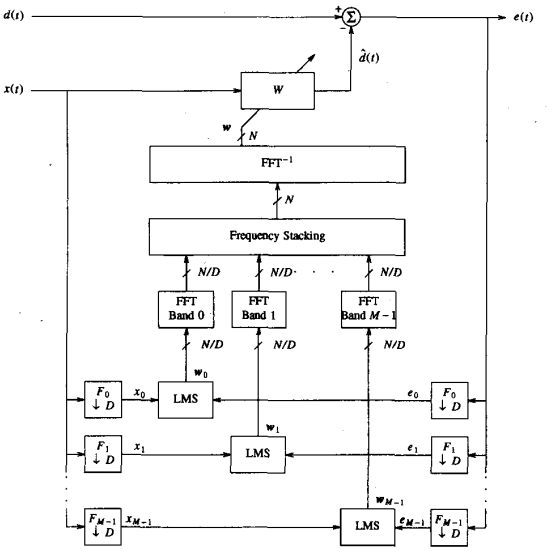

Fig. 3. Delayless subband adaptive filter using the LMS algorithm—Type I (closed loop).

conjugate symmetry. Also, in that case, double-sideband filters could be employed along with the real LMS algorithm, resulting in about twice the number of real weights as complex weights for the former case, but then with real multiplies instead of complex.

We note that the wideband filter convolution can be efficiently computed either by using a vector coprocessor or by using orthogonal transform techniques. A vector coprocessor is a specialized hardware device that is dedicated to fast convolution. Alternatively, fast convolution can be realized using orthogonal transform techniques such as the FFT [3]; however, some care must be taken to insure that no delay is introduced into the signal path. Usually, a fast FFT convolution will entail a block delay in throughput. However, this can be avoided by splitting the wideband filter coefficients into segments of equal length. Then, the first segment can process by direct convolution while the remaining segments process by fast convolutions in time sequence [14],[15]. In that way, the fast convolution part can be started ahead of time by the number of samples in the direct convolution so that the output is available when needed. Thus, the total number of computations for the wideband convolution is reduced by approximately the number of segments (neglecting the fast part of the computation). It is further noted that the FFT's and FFT^{-1}'s need not be performed at the decimated sample rate; a substantial reduction in computation can be realized if they are computed only once every several decimated samples, with a corresponding moderate time lag in convergence. A calculation of the computational requirements will be presented in Section V.

A special case results when direct access to the cancellation summing node in Fig. 1 is available, i.e., when $C = 1$. In that case, the "filtered-x" part is eliminated and the general technique reduces to the delayless subband LMS configuration of Fig. 3. This special case is exemplified by the acoustic echo cancellation problem, where $x(t)$ is an electrical line input signal that drives a loudspeaker, $d(t)$ is the echo signal picked up by the microphone, and the cancellation summing junction is an electronic subtraction circuit that derives the output signal $e(t)$. In this case, the wideband error signal of (1) and subband adaptive weight update of (2) simplify, respectively, to the usual LMS expressions

$$e(t) = d(t) - \boldsymbol{w}^T(t)\boldsymbol{x}(t), t = 0, 1, 2, \cdots \tag{3}$$

and

$$\boldsymbol{w}_m(t + D) = \boldsymbol{w}_m(t) + \mu \boldsymbol{x}_m^*(t) e_m(t), m = 0, 1, \cdots, M - 1 \tag{4}$$

where $\boldsymbol{x}_m(t) \equiv [x_m(t), x_m(t - D), \cdots, x_m(t - N + D)]^T$.

The delayless subband adaptive filters of Figs. 1 and 3 can be characterized as closed-loop systems since the output error is fed back to the subband error filter bank. However, a basic shortcoming of closed-loop systems of this genre is that a delay is introduced into the weight update path, which will limit the convergence rate of the LMS algorithm [16]–[19] as well as the more general FXLMS algorithm [12], [13]. This is of minor concern in some applications, such as active noise control in slowly varying environments. However, in other applications, notably, acoustic echo cancellation, convergence speed is very important, as objects moving in the room cause rapid variations of the echo path impulse response. In that case, an alternative configuration is possible for the special case of Fig. 3, where there is no cancellation path filter. The modified configuration is developed by computing both the error and adaptive weights in subbands, as in a conventional subband adaptive filter, but then transforming the subband weights to an equivalent

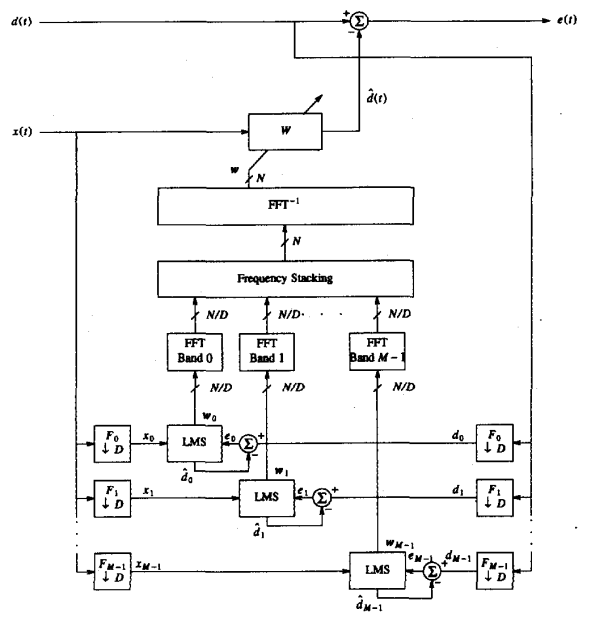

Fig. 4. Delayless subband adaptive filter using the LMS algorithm - Type II (open loop).

wideband filter weight. A block diagram of this second type of delayless subband LMS adaptive filter appears in Fig. 4. In this case, the LMS algorithm, as depicted in Fig. 2(b), also computes a convolution of the subband reference signal

$$\hat{d}_m(t) \equiv \boldsymbol{w}_m^T(t)\boldsymbol{x}_m(t), t = 0, D, 2D, \cdots \tag{5}$$

which is then used to derive a local error signal

$$e_m(t) = d_m(t) - \hat{d}_m(t) \tag{6}$$

where $d_m(t)$ is the mth subband disturbance signal derived from the subband filters. Since the wideband error is not fed back to the subband weight calculation, this can be thought of as an open loop version of Fig. 3.

There is no signal path aliasing for either closed-loop or open-loop versions, since the output signal is not reconstructed from the subband error signals. There is, however, aliasing of the subband signals used to update the adaptive weights. For the closed-loop FXLMS configuration of Fig. 1 as well as the LMS configuration of Fig. 3, any nonzero frequency component of the error will be fed back to the subband adaptive weight update and will have the effect of driving that component to zero. In doing so, aliasing of the subband error signal will slightly perturb the adaptive weights at other frequencies; however, these will also experience closed-loop feedback. Thus, despite aliasing of the reference and error subband signals, the closed-loop delayless adaptive filter will converge to minimum error. For the open-loop LMS version of Fig. 4, there is again no aliasing in the wideband signal path. However, the subband adaptive weights are calculated without the benefit of feedback from the wideband error. Nevertheless, it is shown in Appendix A that even for the open-loop version, the effects of aliasing are greatly diminished relative to the conventional subband adaptive filter.

In practice, it is usually advantageous to normalize the step size to the signal power. Thus, for the normalized FXLMS algorithm

$$\mu = \mu(t) = \frac{\alpha}{\boldsymbol{y}_m^T(t)\boldsymbol{y}_m(t)} \tag{7a}$$

where α is the normalized step size. Similarly, for the LMS algorithm

$$\mu = \mu(t) = \frac{\alpha}{\boldsymbol{x}_m^T(t)\boldsymbol{x}_m(t)}. \tag{7b}$$

Convergence is then assured (almost surely) for $\alpha < 2/3$ as a worst case for a Gaussian process [20]; in practice, normalized step sizes up to a value of about one are commonly used.

III. Polyphase FFT Implementation

One way to implement the delayless subband adaptive filter is to employ the polyphase FFT technique of [21]. This technique realizes M contiguous single-sideband bandpass filters whose outputs are downsampled by a factor $D = M/2$ to produce M complex subband signals. No band shifting is necessary in this case: due to the regular structure, even subbands are centered at dc while odd subbands are centered at one half of the decimated sampling frequency. For real signals, only half of the complex subbands need to be processed, as previously discussed. (Actually, $M/2 + 1$ subband signals $y_0, y_1, \cdots, y_{M/2}$ will be employed.) According to [21], the mth subband reference signal is mathematically expressed as

$$y_m(t) = \sum_{k=0}^{K-1} a_k e^{j2\pi \frac{mk}{M}} y(t-k) \tag{8a}$$

$$= \sum_{n=0}^{M-1} e^{j2\pi \frac{mn}{M}} \sum_{l=0}^{L-1} a_{n+lM} y(t-n-lM) \tag{8b}$$

where a_k are the coefficients of a K-point prototype FIR filter and $K = LM$, where L is an integer. The first form (8a) expresses the convolution of the frequency-shifted prototype filter with the filtered reference signal to obtain a single-sideband subband reference signal. The decomposition $k = n + lM$ obtains the second form (8b), which shows how the (inverse) FFT comes into play, transforming the polyphase filtered reference signals. In the implementation of (8b), two inverse FFT's are staggered and a subband output is produced every $D = M/2$ input samples. Similar expressions describe the subband error signals used for the general FXLMS configuration of Fig. 1 and Type I LMS configuration of Fig. 3, as well as the subband disturbance signals used for the Type II LMS configuration of Fig. 4.

By way of a concrete example, consider the design of an $N = 512$ tap real wideband adaptive filter using $M = 32$ subbands. A 128-tap FIR lowpass filter was designed for the polyphase prototype using the Matlab fir1(127,1/32) routine.

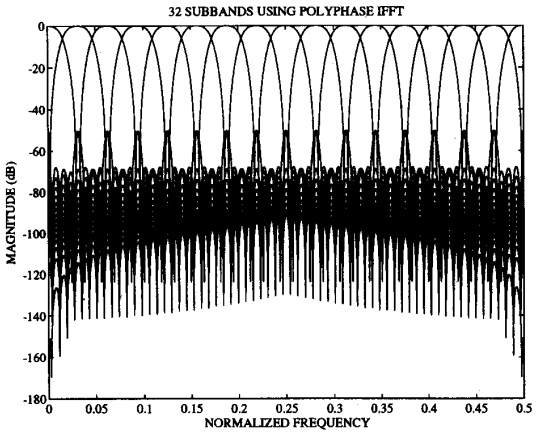

Fig. 5. Frequency response of polyphase FFT filter bank.

(Usually, more sophisticated techniques are employed in the filter design to realize overall flat response [22], [23].) Fig. 5 shows the resulting frequency response of the first $M/2+1 = 17$ filters (which are the only ones processed, due to the complex conjugate symmetry). After decimation by a factor $D = 16$, each subband spans the 512-tap wideband filter using $N/D = 32$ taps per subband. The -70 dB stopband response of the prototype filter insures that the aliasing noise floor will be less than -116 dB for the open-loop configuration (see Appendix A). (As previously argued, the closed-loop configuration will completely nullify a moderate amount of aliasing.) The subband adaptive weights are transformed by 32-point (complex) FFT's to obtain 32 frequencies per subband, which are then stacked as indicated in Fig. 6 and Table I to form points 0–255 of a 512-point array. The array is then completed by setting point 256 equal to zero and using the complex conjugates of points 1–255 in reverse order. Finally, the 512-point array is transformed by a 512-point inverse FFT to obtain the wideband filter weights.

Note that the above example is only for illustration; the general technique can accommodate an arbitrary number of taps, number of subbands, decimation factor, etc., all of which can be optimized for a particular application.

IV. Application Examples

Two applications will now be presented for the polyphase FFT implementation described in the last section. The first will be for an active noise cancellation problem that utilizes the general filtered-x version of Fig. 1. The second application will be for acoustic echo cancellation where the configurations of Figs. 3 and 4 apply.

A. Active Noise Control

As an example of an application of the delayless subband FXLMS technique of Fig. 1, consider the embodiment in Fig. 7. The system in the dashed box represents a plant over which we have no access except for the reference and error observation ports $x(t)$ and $e(t)$, respectively, and the control input that couples through the cancellation path

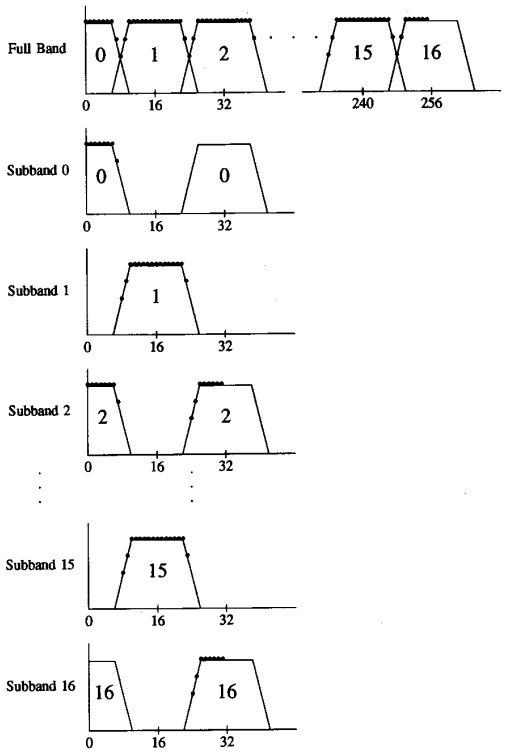

Fig. 6. Example of frequency stacking for 32-subband polyphase FFT implementation with 512-point impulse response and 32 taps per subband.

TABLE I
Frequency Mapping from Suband FFT Bin Number to Wideband FFT Bin Number for 32-Subband Polyphase FFT Implementation with 512-Point Impulse Response and 32 Taps Per Subband

Subband FFT Bin Number	Wideband FFT Bin Number						
	Subband 0	Subband 1	Subband 2	...	Subband 14	Subband 15	Subband 16
0	0	-	32		224	-	-
1	1	-	33		225	-	-
2	2	-	34		226	-	-
3	3	-	35		227	-	-
4	4	-	36		228	-	-
5	5	-	37		229	-	-
6	6	-	38		230	-	-
7	7	-	39		231	-	-
8	-	8	-		-	232	-
9	-	9	-		-	233	-
10	-	10	-		-	234	-
11	-	11	-		-	235	-
12	-	12	-		-	236	-
13	-	13	-		-	237	-
14	-	14	-		-	238	-
15	-	15	-		-	239	-
16	-	16	-		-	240	-
17	-	17	-		-	241	-
18	-	18	-		-	242	-
19	-	19	-		-	243	-
20	-	20	-		-	244	-
21	-	21	-		-	245	-
22	-	22	-		-	246	-
23	-	23	-		-	247	-
24	-	-	24		216	-	248
25	-	-	25		227	-	249
26	-	-	26		218	-	250
27	-	-	27		219	-	251
28	-	-	28		220	-	252
29	-	-	29		221	-	253
30	-	-	30		222	-	254
31	-	-	31		223	-	255

transfer function C to cancel the disturbance signal $d(t)$. The disturbance and reference signals are assumed to be derived

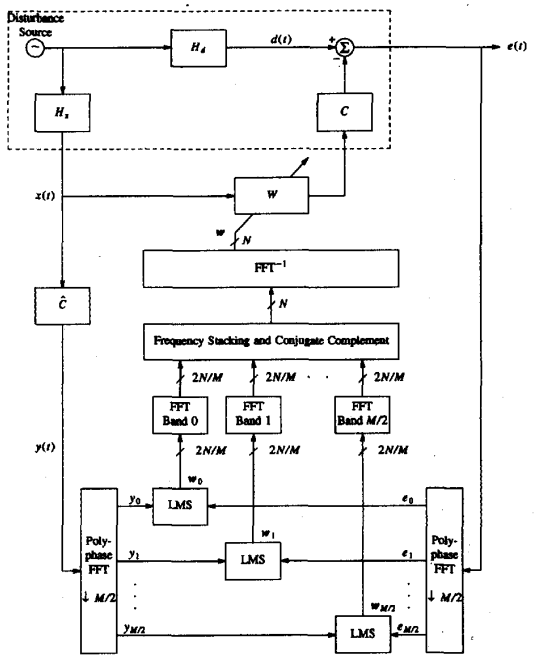

Fig. 7. Delayless subband active noise control using polyphase FFT implementation.

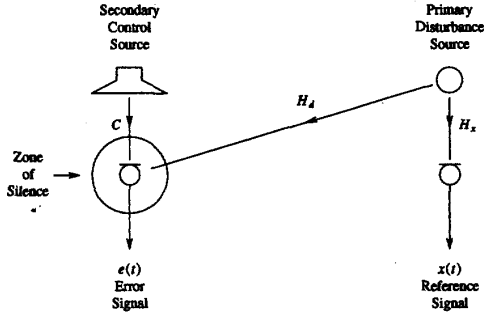

Fig. 8. Schematic diagram of active noise control experiment.

from a common disturbance source through linear transfer functions H_d and H_x, respectively. Since the polyphase FFT implementation is assumed, $M/2+1$ subband signals are depicted using $2N/M$ taps per subband, resulting in N wideband coefficients. Note that the number of wideband coefficients for this application must be sufficient to adequately synthesize the combined response of H_d and $(H_xC)^{-1}$.

Within the above framework, consider the acoustic noise control problem of Fig. 8. A primary disturbance source on the right generates acoustic noise in an enclosed room. It is desired to create a "zone of silence" on the left side by sending a control signal to a loudspeaker that produces a canceling acoustic signal. A microphone on the left obtains the error signal $e(t)$ which is to be minimized. The reference signal $x(t)$ is derived from another microphone on the right, which is in close proximity to the primary disturbance. The various acoustic transfer functions are labeled in accordance with Fig. 7.

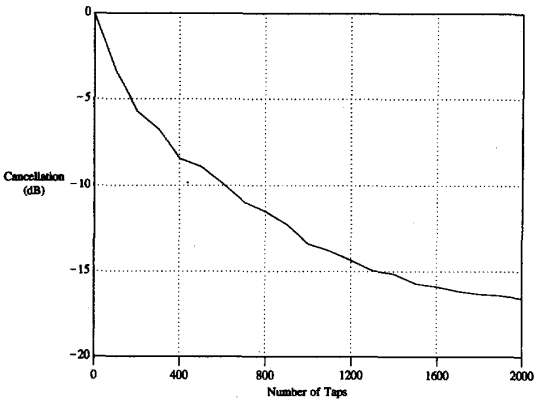

Fig. 9. Theoretical active noise cancellation as a function of number of taps for 100-500 Hz, 10th order bandpass noise.

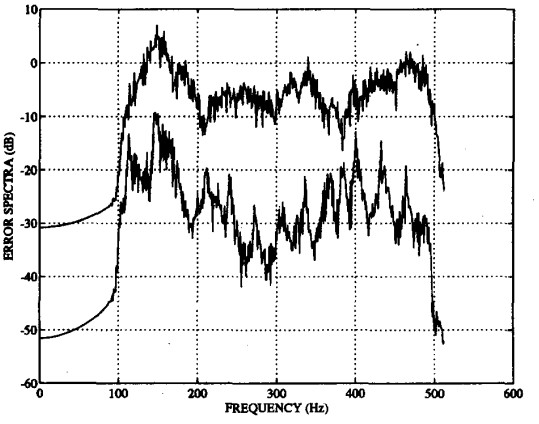

Fig. 10. Error spectra of active noise control computer simulation before and after convergence.

Impulse responses of the transfer functions in Fig. 8 were measured in an actual room (HuMaNet room A [24]) using SYSid [25]. For simplicity, a bandlimited white noise source was assumed over the band 100–500 Hz, which is sampled at 1 kHz. The theoretical minimum error was computed (see Appendix B) using the measured responses and is plotted in Fig. 9 as a function of the number of taps employed for the wideband filter W. As can be seen, several hundred taps are required to realize significant cancellation.

A wideband filter of 512 taps was selected as a compromise between performance and complexity, and used in conjunction with the 32-subband design previously discussed to produce a computer simulation of the above configuration. The room impulse responses were truncated to 256 ms for the purpose of this experiment. (The simulation also assumes that acoustic feedback from the secondary loudspeaker to the reference microphone has been satisfactorily neutralized by other means.) Fig. 10 shows the resulting error spectra before and after convergence. As can be seen, more than 15 dB of cancellation is achieved over most of the band; the overall performance is dominated by the cancellation around 150 Hz and 400 Hz, the result being in rough agreement with the

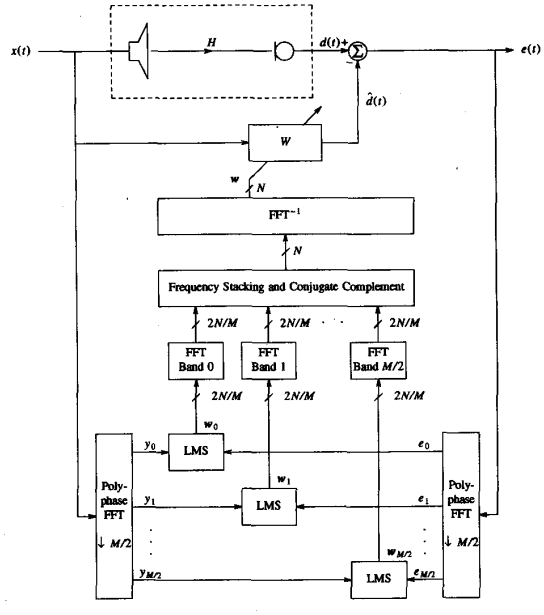

Fig. 11. Delayless subband echo canceler using polyphase FFT implementation—Type I (closed loop).

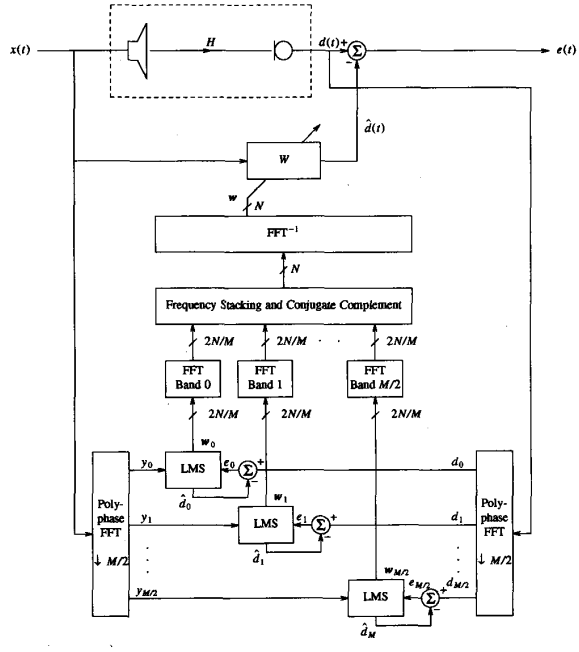

Fig. 12. Delayless subband echo canceler using polyphase FFT implementation—Type II (open loop).

9 dB level predicted from Fig. 9 for 512 taps. These results demonstrate the viability of the delayless subband technique for active noise control.

B. Acoustic Echo Cancellation

Now, an application of the delayless subband LMS algorithm of Figs. 3 and 4 will be illustrated for acoustic echo cancellation. Figs. 11 and 12 show the general configuration for closed-loop and open-loop versions, respectively, where now $x(t)$ is interpreted as the far-end received signal which drives a loudspeaker, H is the acoustic echo path transfer function to the microphone signal $d(t)$, and $e(t)$ is the de-echoed return signal (to which the desired near-end signal is added). An $N = 512$-point wideband impulse response was assumed with an 8 kHz sampling rate and the 32-subband design previously discussed was used in a computer simulation with a measured room acoustic impulse response. For this example, the wideband filter was updated every $N/4 = 128$ samples. Fig. 13 shows the convergence of the echo return loss (ERL) as a function of time with a normalized step size $\alpha = 0.3$ (the ERL was computed by smoothing both $e^2(t)$ and $d^2(t)$ using a first order filter with decay factor 0.95 and then taking the ratio). The closed-loop configuration (solid line) converges at a steady rate to the misadjustment noise floor, which was measured at -78 dB for this example; aliasing effects, which are theoretically completely nullified (see Appendix A), were measured at less than -140 dB using very small step sizes. In contrast, the open-loop configuration (dotted line) converges slightly faster initially, but then appears to reach a -30 dB limit. Actually, in this case, the convergence has not reached the misadjustment or aliasing noise floor (measured at -35 and -72 dB, respectively), but is in a state of slow asymptotic convergence due to the small eigenvalues associated with the band edges of the subband filters [26]; this behavior is common for LMS adaptive filters involving wideband signals with bandlimiting filters. Although the closed-loop version converges somewhat slower initially (because of the delay in the wideband filter update), the common error feedback prevents capture by slow asymptotic modes: for any arbitrary frequency component of the error, there will be a corresponding strong frequency component in one of the subband reference signals, thereby enabling rapid cancellation of that component. An obvious melding of the two versions could be realized by switching configurations when the ERL reaches a certain level, say -20 dB for this example. Alternatively, it may be possible to eliminate slow asymptotic convergence for the open-loop configuration by postfiltering [26]; research is in progress to examine this possibility [27]. Another approach would be to reduce the convergence lag of the closed-loop version by updating the wideband filter more often; updating every $N/8 = 64$ samples produces initial convergence nearly identical to the open-loop case.

V. Computational Requirements

The computational requirements of the delayless active noise control algorithm can be separated into four parts: 1) subband filtering, 2) adaptive weight update, 3) subband/wideband weight transformation, and, 4) signal path convolution associated with the wideband filter W. The first two requirements are similar to those for conventional subband acoustic echo cancellation, whereas the last two pertain to the proposed delayless subband configuration. For convenience, the computational complexity here will be based only on the number of multiplies per input sample; the relative comparisons should

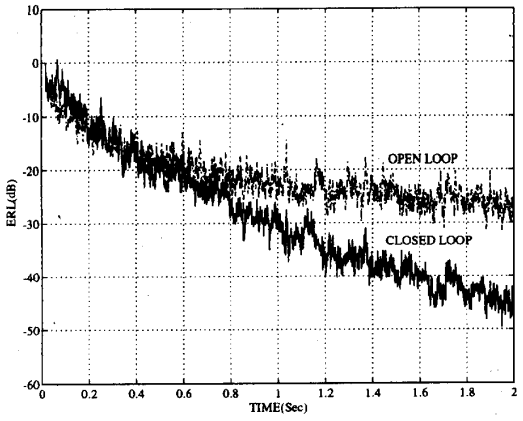

Fig. 13. Echo return loss (ERL) convergence for open-loop and closed-loop delayless subband echo canceler; normalized step size, $\alpha = 0.3$.

also roughly hold for other measures. Also, the calculations here assume use of the polyphase FFT approach of Section III with real input and output signals; other implementations of the basic concept may prove even more advantageous.

For M subbands, the $2\times$ oversampled polyphase FFT subband filtering technique [21] requires one K-tap prototype filter convolution and one M-point real FFT for each batch of $M/2$ input samples. An M-point real FFT requires about $M\log_2 M$ real multiplies. Therefore, the subband filtering requires

$$R_1 = 2K/M + 2\log_2 M \tag{9}$$

real multiplies per input sample.

Due to the spectral conjugate symmetry of real signals, it is only necessary to process half of the M complex subband signals. Since the subband filter outputs are downsampled by a factor $D = M/2$, each of the $M/2$ lower subbands has to update $2N/M$ complex adaptive weights every $M/2$ input samples. Therefore the weight update for the closed-loop version entails

$$R_2 = 8N/M \tag{10}$$

real multiplies per input sample. For the open-loop version, an additional R_2 real multiplies per sample are required to implement the subband signal path convolutions (5).

The weight transformation requires a $2N/M$-point complex FFT for each of the $M/2$ lower subbands and an N-point inverse real FFT. A $2N/M$-point complex FFT requires about $4N/M\log_2(2N/M)$ real multiplies. However, since the wideband filter output cannot change much faster than the length of its impulse response, it is only necessary to perform the wideband weight transformations every N/J input samples, where J is typically in the range one to eight. Thus

$$R_3 = [2\log_2(2N/M) + \log_2 N]J \tag{11}$$

real multiplies per input sample. The update rate is more critical for the closed-loop version since the delay affects the weight convergence in that case; for the open-loop version, the wideband error is not used in the weight update and the error convergence is simply shifted by N/J samples

The signal path convolution is performed by dividing the total number of N coefficients into L segments, giving $N_s = N/L$ taps per segment. The first segment is processed with direct convolution, which therefore requires N_s real multiplies per input sample. The remaining $L-1$ segments are processed using fast convolution [14], [15], which for each block of N_s samples requires one $2N_s$-point real FFT for the input signal, $L-1$ $2N_s$-point real FFT's for the adaptive weights, $(L-1)N_s$ (frequency domain) complex multiplies, and one $2N_s$-point inverse real FFT. Thus

$$\begin{aligned} R_4 &= N_s + 2L\log_2(2N_s) + 4(L-1) + 2\log_2(2N_s) \\ &= N/L + 2(L+1)\log_2(2N/L) + 4(L-1) \end{aligned} \tag{12}$$

real multiplies per input sample. This rate can be compared to conventional direct convolution, which would require $R_4' = N$ real multiplies per input sample. This method of delayless fast convolution then requires a fraction

$$\frac{R_4}{R_4'} = \frac{1}{L} + \frac{2(L+1)\log_2(2N/L) + 4(L-1)}{N} \tag{13}$$

that of direct convolution. For any given number of wideband filter coefficients N, the number of segments L can be optimized for achieving a minimum rate. For example, with $N = 512$ coefficients, R_4/R_4' is minimized at 0.41 for $L = 6$ segments, i.e., a reduction of about 60%.

Putting it all together then finally results in the total computational rate

$$R_{\text{closed}} = R_1 + R_2 + R_3 + R_4 \tag{14}$$

for the closed-loop delayless subband algorithm and

$$R_{\text{open}} = R_1 + 2R_2 + R_3 + R_4 \tag{15}$$

for the open-loop version.

For the examples considered in this paper, there are $N = 512$ fullband taps, $M = 32$ subbands, and a $K = 128$ tap prototype filter. Therefore, the above expressions evaluate to $R_1 = 18$, $R_2 = 128$, $R_3 = 19J$. Also, for $L = 8$ segments, which is near-optimal, $R_4 = 218$. If the wideband filter is updated every $N = 512$ samples ($J = 1$), the total rate for the closed-loop delayless subband algorithm evaluates to $R_{\text{closed}} = 383$ real multiplies per input sample. This rate can be compared to the conventional LMS algorithm, which would require 1024 multiplies per sample for $N = 512$ taps. Thus, for this example, the closed-loop delayless subband technique reduces the computational load to about one third that of the conventional fullband LMS algorithm. For some applications requiring fast convergence, it is necessary to update the wideband filter more often and R_3 will accordingly increase by the factor J. For the acoustic echo cancellation example of Fig. 13, the wideband filter was updated every $N/4 = 128$ samples ($J = 4$) and that would increase R_3 from 19 to 76, which is not a severe penalty.

For the open-loop version, R_2 is doubled and the rate increases to $R_{\text{open}} = 511$ real multiplies per input sample for $J = 1$. However, when fast convergence is necessary, this rate

increase is offset somewhat by the fact that the wideband filter does not have to be updated as often as for the closed-loop version. For the example of Fig. 13, there was no noticeable difference for the open-loop case when the update time was increased to 512 samples ($J = 1$).

By way of comparison, a conventional subband LMS algorithm using the same subband filter implementation with a 128-point linear-phase FIR prototype filter would result in an overall delay of 128 samples for the combined analysis and synthesis filters, which corresponds to 16 ms at an 8kHz sampling rate. Like the open-loop delayless subband algorithm, this conventional subband LMS algorithm would require R_1 and $2R_2$ real multiplies per sample for the subband filtering, adaptive weight update, and subband signal path convolutions. However, instead of R_3 and R_4, the conventional subband output convolutions would only entail another R_1 real multiplies per sample for the synthesis filtering. Overall, a total of $2R_1 + 2R_2$ real multiplies per sample would then be required. For the same numbers as above, this works out to a rate of 292 real multiplies per sample, which can be compared to 383 for the closed-loop delayless subband LMS algorithm and 511 for the open-loop version (both for $J = 1$). Thus, the delayless subband LMS algorithm retains most of the computational efficiency of the conventional subband LMS algorithm while eliminating all signal path delay.

VI. Conclusion

A new type of subband adaptive filter has been described that retains the computational and convergence speed advantages of subband processing, while eliminating any delay in the signal path. This technique has applications in active noise control, where delay seriously limits cancellation performance, and acoustic echo cancellation, where transmission delay specifications now limit the use of efficient subband designs. The delayless subband adaptive filter is applicable to both LMS and, more generally, FXLMS applications. For the LMS version, two configurations are possible: closed-loop and open-loop. Each has certain advantages and may be best employed together in a switchable configuration.

A further advantage of the delayless configuration is that there is no aliasing in the signal path. This results in complete nullification of subband aliasing effects for the closed-loop configuration. The open-loop version, while not completely immune to subband aliasing, still substantially reduces the effects from those experienced conventionally. As a result, more efficient subband filters could be designed by relaxing the low stopband response necessary to control aliasing.

One particularly efficient method for realizing the delayless subband adaptive filter uses polyphase FFT subband filters. A design example was developed for a 512-tap wideband adaptive filter using 32 subbands. Application examples were presented for active acoustic noise control and acoustic echo cancellation using numerical simulations with actual measured impulse responses.

For the 512-tap, 32-subband design example, the computational load of the polyphase FFT subband implementation was shown to be only about one third that of a conventional fullband design. Alternatively, for a given computational load, the proposed subband design affords an adaptive filter length about three times as long as the conventional wideband design. A further enhancement of computational efficiency can be realized using more subbands with correspondingly higher decimation rate, albeit with an increased lag in convergence.

It is also possible to realize the delayless subband adaptive filter using double-sideband subband filters to derive real subband signals; this involves a number of real weights that is about twice the number of complex weights for complex subband signals, but then only real instead of complex multiplies are required. Efficient implementations of this approach could also employ fast real transforms, such as the discrete cosine transform (DCT).

Appendix A
Calculation of Aliasing Effects

In this appendix, the effects of aliasing introduced by subband decimation will be examined for both conventional and the new delayless subband adaptive filter. For simplicity, it will be assumed that the reference signal x is a white noise random process and that the plant frequency response is a realization of a random ensemble with unit-power Rayleigh statistics that are independent over frequency.

A. Conventional Subband Adaptive Filter

Consider the cancellation of a component at frequency f_0 in subband 0 and let $f_1, f_2, \cdots, f_{D-1}$ denote frequencies in the $D-1$ subbands that alias to f_0 when the subband signals are decimated. Further, let $\epsilon_1, \epsilon_2, \cdots, \epsilon_{D-1}$ denote the complex subband filter response at these frequencies and define the average magnitude-squared stopband response

$$\epsilon^2 \equiv \frac{1}{D-1} \sum_{i=1}^{D-1} |\epsilon_i|^2 \tag{A1}$$

which is a small number by design. Then the aliased reference signal at frequency f_0 will comprise independent components with complex amplitudes $1, \epsilon_1, \epsilon_2, \cdots, \epsilon_{D-1}$. The aliased disturbance signal of subband 0 will have corresponding components $H_0, H_1\epsilon_1, H_2\epsilon_2, \cdots, H_{D-1}\epsilon_{D-1}$, where H_i is the plant frequency response at frequency f_i. The Rayleigh fading assumption characterizes the statistics of H_i as zero-mean, independent random variables:

$$E\{H_i\} = 0 \tag{A2a}$$

$$E\{H_i H_j^*\} = \begin{cases} 0, i \neq j \\ 1, i = j \end{cases}. \tag{A2b}$$

Denote the equivalent adaptive weight at frequency f_0 as W and write the corresponding error component at that frequency as

$$E_0 = (H_0 - W) + (H_1 - W)\epsilon_1 + (H_2 - W)\epsilon_2 + \cdots$$
$$\cdots + (H_{D-1} - W)\epsilon_{D-1}. \tag{A3}$$

Since the aliased frequency components are statistically independent, the expected error power over the reference signal

ensemble is expressed as

$$E_x\{|E_0|^2\} = |H_0 - W|^2 + |H_1 - W|^2|\epsilon_1|^2 + \cdots + |H_{D-1} - W|^2|\epsilon_{D-1}|^2. \quad \text{(A4)}$$

Quadratic forms of a complex variable W can be minimized by pretending that W and its complex conjugate W^* are independent variables and setting the derivative with respect to one of them equal to zero [28]. Thus, expanding (A4) in terms of W and W^* and differentiating with respect to W^* obtains the optimal weight

$$W_{\text{opt}} = \frac{H_0 + H_1|\epsilon_1|^2 + \cdots + H_{D-1}|\epsilon_{D-1}|^2}{1 + |\epsilon_1|^2 + \cdots |\epsilon_{D-1}|^2} = \frac{H_0 + H_1|\epsilon_1|^2 + \cdots + H_{D-1}|\epsilon_{D-1}|^2}{1 + (D-1)\epsilon^2}. \quad \text{(A5)}$$

For the conventional subband adaptive filter, the output is synthesized from all of the subband error signals. Thus, substituting (A5) into (A4) and neglecting terms of order $|\epsilon_i|^4$ gives

$$E_x\{|E_0|^2\}_{\min} \approx \frac{|H_1 - H_0|^2|\epsilon_1|^2 + \cdots + |H_{D-1} - H_0|^2|\epsilon_{D-1}|^2}{[1 + (D-1)\epsilon^2]^2}. \quad \text{(A6)}$$

Now, the overall expected value of (A6) is calculated using the independent Rayleigh statistics (A2), resulting in the aliasing noise floor

$$\sigma^2_{\text{conv}} \equiv E\{|E_0|^2\}_{\min} = E_H E_x\{|E_0|^2\}_{\min} \approx \frac{2(D-1)\epsilon^2}{[1 + (D-1)\epsilon^2]^2}. \quad \text{(A7)}$$

Since it is usually desired to make this a small quantity, the denominator can be neglected, giving finally,

$$\sigma^2_{\text{conv}} \approx 2(D-1)\epsilon^2. \quad \text{(A8)}$$

As an example, for $D = 16$ and $\epsilon^2 = 10^{-7}$ (-70 dB), (A8) gives an aliasing noise floor of 3×10^{-6} (-55 dB).

B. Delayless Subband Adaptive Filter

For the delayless subband adaptive filter, the output signal is not reconstructed from the subband error signals but is formed by an auxiliary wideband filter whose coefficients are derived from the subband adaptive weights. Hence, there is no signal path aliasing. However, there is aliasing of the subband signals used to update the adaptive weights. These effects will now be discussed for the closed-loop and open-loop versions of the delayless subband adaptive filter developed in the main text. The closed-loop version applies to the FXLMS configuration of Fig. 1 as well as the LMS configuration of Fig. 3, while the open-loop version applies exclusively to the LMS configuration of Fig. 4.

For the closed-loop delayless subband adaptive filter, any nonzero frequency component of the error will be fed back to the subband adaptive weight update and will have the effect of driving that component to zero. In doing so, aliasing of the subband error signal will slightly perturb the adaptive weights at other frequencies, however, these will also experience closed-loop feedback. Thus, despite aliasing of the reference and error subband signals, the closed-loop delayless adaptive filter will converge to zero error:

$$\sigma^2_{\text{closed}} \to 0. \quad \text{(A9)}$$

Now consider the open-loop delayless adaptive filter. Again, there is no aliasing in the wideband signal path. However, the subband adaptive weights are calculated without the benefit of feedback from the wideband error. Therefore, the subband adaptive weight at frequency f_0 in subband zero will be perturbed by subband signal aliasing in the same manner as for the conventional subband adaptive filter, viz. (A5). In the frequency domain, there is a direct correspondence between the effective frequency-domain weights of the wideband and subband filters. Thus, the output error signal for a given plant frequency response realization is expressed as

$$E_x\{|H_0 - W_{\text{opt}}|^2\} = \left|\frac{H_0(D-1)\epsilon^2 - H_1|\epsilon_1|^2 - \cdots - H_{D-1}|\epsilon_{D-1}|^2}{1 + (D-1)\epsilon^2}\right|^2. \quad \text{(A10)}$$

Again, application of the Rayleigh statistics (A2) determines the aliasing noise floor

$$\sigma^2_{\text{open}} \equiv E\{|H_0 - W_{\text{opt}}|^2\} = \frac{(D-1)^2\epsilon^4 + |\epsilon_1|^4 + \cdots + |\epsilon_{D-1}|^4}{[1 + (D-1)\epsilon^2]^2}. \quad \text{(A11)}$$

For the special case when $|\epsilon_i| = \epsilon$ (equiripple stopband response) and $(D-1)\epsilon^2 \ll 1$, (A11) becomes simply

$$\sigma^2_{\text{open}} \approx D(D-1)\epsilon^4. \quad \text{(A12)}$$

Comparing this with (A8) shows that the open-loop delayless subband adaptive filter results in an aliasing noise floor that is of order ϵ^4, as compared to order ϵ^2 for the conventional subband adaptive filter. For the same example as before with $D = 16$ and $\epsilon^2 = 10^{-7}$ (-70 dB), (A12) gives an aliasing noise floor of 2.4×10^{-12} (-116 dB). This can be compared to the -55 dB realized by the conventional subband adaptive filter.

Thus, the delayless subband adaptive filter is much more tolerant of aliasing than the conventional configuration. This fact could be used to design more efficient subband filters by relaxing the requirement for low stopband response.

APPENDIX B
THEORETICAL MINIMUM MEAN-SQUARE ERROR FOR ACTIVE NOISE CONTROL

In this appendix, a mathematical expression will be developed for the theoretical minimum mean-square error of a generic active noise control system. A block diagram of the basic setup is shown in Fig. 14. The system in the dashed box represents a plant over which we have no access except for the reference and error observation ports $x(t)$ and $e(t)$,

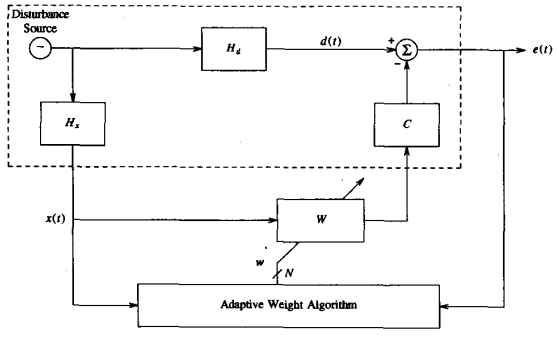

Fig. 14. Block diagram of generic active noise control system.

respectively, and the control input that couples through the cancellation path transfer function C to cancel the disturbance signal $d(t)$. The disturbance and reference signals are assumed to be derived from a common disturbance source through linear transfer functions H_d and H_x, respectively. The control algorithm adjusts the coefficients comprising the N-tap FIR filter W in order to minimize the residual error $e(t)$ in a mean-square sense. The number of coefficients N must be sufficient to adequately synthesize the combined response of H_d and $(H_xC)^{-1}$. The following development will formulate the minimum mean-square error, which can then be evaluated as a function of N.

Assuming that the adaptive weight vector varies much slower than the reference signal, the error signal can be written as

$$e(t) = d(t) - \boldsymbol{w}^T\boldsymbol{y}(t) \tag{B1}$$

where $d(t)$ is the disturbance signal, $\boldsymbol{w}$ is a vector of N adaptive weights with superscript T denoting transpose, and

$$\boldsymbol{y}(t) \equiv c(t) * \boldsymbol{x}(t) \tag{B2}$$

is the filtered reference signal vector, where $c(t)$ is the impulse response of the cancellation path, $*$ denotes convolution, and $\boldsymbol{x}(t) \equiv [x(t), x(t-1), \cdots, x(t-N+1)]^T$ is a vector comprising the N most recent reference samples. Squaring (B1) and taking the expected value then gives

$$\xi \equiv E\{e^2(t)\} = \sigma_d^2 - 2\boldsymbol{w}^T\boldsymbol{r} + \boldsymbol{w}^T\boldsymbol{R}\boldsymbol{w} \tag{B3}$$

where $\sigma_d^2 \equiv E\{d^2(t)\}$ is the disturbance signal power,

$$\boldsymbol{r} \equiv E\{d(t)\boldsymbol{y}(t)\} \tag{B4}$$

is the cross-correlation vector between the disturbance d and the filtered reference vector $\boldsymbol{y}$, and

$$\boldsymbol{R} \equiv E\{\boldsymbol{y}\boldsymbol{y}^T\} \tag{B5}$$

is the covariance matrix of the filtered reference vector $\boldsymbol{y}$; the components of the above are expressed

$$r_n = E\{d(t)y(t-n)\} \equiv R_{dy}(n),\ n = 0, 1, \cdots, N-1 \tag{B6}$$

and

$$R_{nm} = E\{y(t-n)y(t-m)\} \equiv R_{yy}(m-n),\ n, m = 0, 1, \cdots, N-1 \tag{B7}$$

where R_{dy} and R_{yy} are the respective crosscorrelation and autocorrelation functions. These functions can be expressed in terms of frequency-domain entities as

$$R_{dy}(n) = F^{-1}\{H_d(f)H_x^*(f)C^*(f)S_{uu}(f)\} \tag{B8}$$

and

$$R_{yy}(n) = F^{-1}\{|H_x(f)C(f)|^2 S_{uu}(f)\} \tag{B9}$$

where F^{-1} denotes inverse discrete Fourier transform and S_{uu} is the power spectrum of the disturbance source.

Differentiating (B3) with respect to $\boldsymbol{w}$ and equating to zero gives the optimal weight vector

$$\boldsymbol{w}_{\text{opt}} = \boldsymbol{R}^{-1}\boldsymbol{r} \tag{B10}$$

which results in the minimum mean-square error

$$\xi_{\min} = \sigma_d^2 - \boldsymbol{r}^T\boldsymbol{w}_{\text{opt}}. \tag{B11}$$

ACKNOWLEDGMENT

The authors wish to express their thanks to D. Berkley and M. Sondhi for helpful discussion of the ideas developed in this work. Thanks also go to J. Schroeter and D. Duttweiler for careful reading of an early draft and providing many useful comments.

REFERENCES

[1] B. Widrow and S. D. Stearns, *Adaptive Signal Processing*. Englewood Cliffs, NJ: Prentice-Hall, 1985.
[2] P. A. Nelson and S. J. Elliott, *Active Control of Sound*. New York: Academic Press, 1992.
[3] J. J. Shynk, "Frequency-domain and multirate adaptive filtering," *IEEE Signal Processing Mag.*, vol. 9, pp. 14–37, Jan. 1992.
[4] M. M. Sondhi and W. Kellermann, "Adaptive echo cancellation for speech signals," in *Advances in Speech Signal Processing*, S. Furui and M. M. Sondhi, Eds. New York: Marcel Dekker, 1992, ch. 11.
[5] P. J. VanGerwen, F. A. M. van de Laar, and J. J. Kotmans, "Digital echo canceller," U.S. Patent 4,903,247, Feb. 20, 1990 (filed June 23, 1988).
[6] J. M. Cioffi and J. A. C. Bingham, "A data-driven multitone echo canceller," in *Proc. IEEE GLOBECOM '91*, 1991, pp. 2.4.1–2.4.5.
[7] D. R. Morgan, "An analysis of multiple correlation cancellation loops with a filter in the auxiliary path," *IEEE Trans. Acoust., Speech, Signal Processing*, vol. ASSP-28, pp. 454–467, Aug. 1980.
[8] J. C. Burgess, "Active sound control in a duct: A computer simulation," *J. Acoust. Soc. Amer.*, vol. 70, pp. 715–726, Sept. 1981.
[9] B. Widrow, D. Shur, and S. Shaffer, "On adaptive inverse control," in *Proc. 15th Asilomar Conf. Circuits, Syst., Comput.*, 1981, pp. 185–189.
[10] S. J. Elliott, I. M. Stothers, and P. A. Nelson, "A multiple error LMS algorithm and its application to the active control of sound and vibration," *IEEE Trans. Acoust., Speech, Signal Processing*, vol. ASSP-35, pp. 1423–1434, Oct. 1987.
[11] L. J. Eriksson, "Development of the filtered-U algorithm for active noise control," *J. Acoust. Soc. Amer.*, vol. 89, pp. 257–265, Jan. 1991.
[12] D. R. Morgan and C. Sanford, "A control theory approach to the stability and transient analysis of the filtered-x LMS adaptive notch filter," *IEEE Trans. Signal Processing*, vol. 40, pp. 2341–2346, Sept. 1992.
[13] D. R. Morgan and J. Thi, "A multi-tone pseudo-cascade filtered-x LMS adaptive notch filter," *IEEE Trans. Signal Processing*, vol. 41, pp. 946–956, Feb. 1993.

[14] M. Xu and Y. Grenier, "Time-frequency domain adaptive filter," in *Proc. IEEE Int. Conf. Acoust., Speech, Signal Processing*, 1989, pp. 1154–1157.
[15] J. M. P. Borallo and M. G. Otero, "On the implementation of a partitioned block frequency domain adaptive filter (PBFDAF) for long acoustic echo cancellation," *Signal Processing*, vol. 27, pp. 301–315, June 1992.
[16] P. Darlington and S. J. Elliott, "Synchronous adaptive filters with delayed coefficient adaption," in *Proc. IEEE Int. Conf. Acoust., Speech, Signal Processing*, 1988, pp. 2586–2589.
[17] G. Long, F. Ling, and J. G. Proakis, "The LMS algorithm with delayed coefficient adaptation," *IEEE Trans. Acoust., Speech, Signal Processing*, vol. 37, pp. 1397–1405, Sept. 1989.
[18] R. Haimi-Cohen, H. Herzberg, and Y. Be'ery, "Delayed adaptive LMS filtering: current results," in *Proc. IEEE Int. Conf. Acoust., Speech, Signal Processing*, 1990, pp. 1273–1276.
[19] G. Long, F. Ling, and J. G. Proakis, "Correction to 'The LMS algorithm with delayed coefficient adaptation,'" *IEEE Trans. Signal Processing*, vol. 40, pp. 230–232, Jan. 1992.
[20] A. Feuer and E. Weinstein, "Convergence analysis of LMS filters with uncorrelated Gaussian data," *IEEE Trans. Acoust., Speech, Signal Processing*, vol. ASSP-33, pp. 222–230, Feb. 1985.
[21] E. R. Ferrara, Jr., "Frequency-domain adaptive filtering," in *Adaptive Filters*, C. F. N. Cowan and P. M. Grant, Eds. Englewood Cliffs, NJ: Prentice-Hall, 1985, ch. 6, pp. 145–179.
[22] G. Wackersreuther, "Some new aspects of filters for filter banks," *IEEE Trans. Acoust., Speech, Signal Processing*, vol. ASSP-34, pp. 1182–1200, Oct. 1986.
[23] P. P. Vaidyanathan, *Multirate Systems and Filter Banks*. Englewood Cliffs, NJ: Prentice-Hall, 1993.
[24] D. A. Berkley and J. L. Flanagan, "HuMaNet: An experimental human-machine communications network based on ISDN wideband audio," *AT&T Tech. J.*, vol. 69, pp. 87–99. Sept./Oct. 1990.
[25] *User's Manual for the SYSid Audio-Band Measurement and Analysis System Version 4.0*, Highland Park, NJ: Ariel Corporation, 1992.
[26] D. R. Morgan, "Slow asymptotic convergence of LMS acoustic echo cancelers," *IEEE Trans. Speech Audio Processing*, vol. 3, pp. 126–136, Mar. 1995.
[27] P. L. DeLeon and D. M. Etter, "Experimental results with increased bandwidth analysis filters in oversampled, subband acoustic echo cancellers," *IEEE Signal Processing Lett.*, vol. 2, pp. 1–3, Jan. 1995.
[28] D. H. Brandwood, "A complex gradient operator and its application in adaptive array theory," *Proc. IEE*, vol. 130, Pts. F and H, pp. 11–16, Feb. 1983.

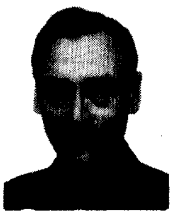

Dennis R. Morgan (S'63–M'69–SM'92) was born in Cincinnati, OH, on February 19, 1942. He received the B.S. degree in 1965 from the University of Cincinnati, OH, and the M.S. and Ph.D. degrees from Syracuse University, Syracuse, NY, in 1968 and 1970, respectively, all in electrical engineering.

From 1965 to 1984, he was with the General Electric Company, Electronics Laboratory, Syracuse, NY, specializing in the analysis and design of signal processing systems used in radar, sonar, and communications. He is now a Distinguished Member of Technical Staff at AT&T Bell Laboratories, where he has been employed since 1984. From 1984 to 1990, he was with the Special Systems Analysis Department, Whippany, NJ, where he was involved in the analysis and development of advanced signal processing techniques associated with communications, array processing, detection and estimation, and adaptive systems. Since 1990, he has been with the Acoustics Research Department, Murray Hill, NJ, where he is engaged in research on adaptive acoustic signal processing techniques.

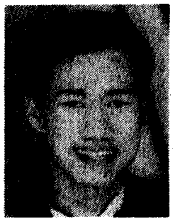

James C. Thi (S'82–M'84) was born in Saigon, Vietnam, on March 18, 1958. He received the B.S. degree in bioengineering from the University of California, San Diego, in 1980 and the M.S. and Ph.D. degrees in electrical engineering from the University of California, Irvine, in 1981 and 1986, respectively.

From 1986 to 1988, he was employed with Northrop, Electronic Division, El Segundo, CA. From 1988 to 1994, he was with the Special Systems Analysis Department of AT&T Bell Laboratories, Arlington, VA, where he was involved in the analysis and design of adaptive signal processing algorithms used in communications systems. Since 1994, he has been with Rockwell International, Newport Beach, CA.